

# Lifetime and Failure Mechanisms of an Arrayed Carbon Nanotube Field Emission Cathode

Logan T. Williams, *Member, IEEE*, Victor S. Kumsomboone, W. Jud Ready, *Senior Member, IEEE*, and Mitchell L. R. Walker

**Abstract**—There is interest in the use of carbon nanotubes (CNTs) to create a field emission (FE) cathode for the neutralization of exhaust plumes of low-power (< 500 W) electric propulsion devices since FE cathodes do not require a gas flow to operate. To incorporate CNT emitters into propulsion systems, the current emission output over the lifetime of the cathode must be understood. Multiple FE cathodes that consist of multiwalled CNT arrays have been fabricated. Seven cathodes are characterized at pressures below  $10^{-5}$  T at constant voltage between the CNTs, and the gate until failure occurs. The maximum current density observed is  $9.08 \text{ mA/cm}^2$  with average current densities up to  $2.52 \text{ mA/cm}^2$ , and the maximum life span is 368 h. The behavior of the cathode current emission is highly unstable and consists of oscillations and sudden shifts. Resistive heating is believed to be the primary cause for failure in two thermally assisted modes: 1) oxidative ablation at the root of the nanotube and 2) field evaporation at the tip.

**Index Terms**—Carbon nanotube (CNT), failure mechanism, field emission (FE) cathode, lifetime.

## I. INTRODUCTION

THE USE of carbon nanotubes (CNTs) for field emission (FE) cathodes holds great potential as a general electron emitter, particularly in the area of electric propulsion (EP). There is a need for a steady long-life (2000 h) efficient electron source to neutralize the exhaust plume of low-power EP devices (< 500 W) [1]. Most thrusters operate in conjunction with thermionic hollow cathodes, which require a gas flow of up to 10% of the total propellant flow in order to efficiently emit electrons [2]. An FE cathode also requires fewer power sources to operate, making it a simpler setup and, thus, an attractive alternative. Beyond the systems design advantages, FE cathodes are very durable, as CNTs are both chemically and mechanically robust [3]. Recent work shows the potential of FE cathodes in the areas of not only low-power EP but also propellantless propulsion, such as space tethers and spacecraft charge control [1], [4].

FE is the extraction of electrons from a conductive material through quantum tunneling. The application of an external

electric field lowers the potential barrier to the point that the transmission probability of an electron becomes nonnegligible. FE devices share the common feature that the emission sites are small points, which focus the electric field and increase the local electric field strength. This focusing effect allows for low macroscopic electric field strengths ( $\sim 1 \text{ V}/\mu\text{m}$ ) to enable electron emission. This focusing effect is quantified by the field enhancement factor.

Past designs of FE cathodes consist of a base material, which is, generally, a doped n-type semiconductor, with a layer of emitter material on top. A conductive screen or mesh, which is termed the gate, placed above the emitter is the extraction electrode. The electric field is generated between the emitter material and the gate. Spindt developed the first FE cathodes in the late 1960s, which used metal cones as the emitter material. Subsequent FE cathode designs use different emitter materials, including films made from diamond and CNTs [3], [5]–[9]. This paper studies the current emission of seven CNT cathodes with a constant voltage applied between the CNTs and the gate to investigate the current emission over time and the failure mechanism of the device.

## II. EXPERIMENTAL DESIGN

### A. Cathode Design and Fabrication

The cathode fabrication process consists of successive layer deposition. The base is a wafer of n-type silicon that is  $420 \mu\text{m}$  thick. An insulator layer of silica ( $\text{SiO}_2$ ) is thermally grown  $10 \mu\text{m}$  thick atop the silicon. The gate layer is formed by the deposition of a 250-nm-thick layer of chromium with electron beam evaporation. A layer of photoresist is deposited with a pattern of a repeated shape formed by photolithography, which defines the shape of the nanotube arrays. The array patterns have a shape size (such as length or diameter as appropriate) and pitch (the separation distance between the centers of adjacent arrays). The array geometry of each sample is outlined in Table I. After the pattern is developed, the gate is etched away via a standard chromium etch process, and the  $\text{SiO}_2$  insulator is etched via reactive ion etching. Since the etch rate differs between the two materials, more of the silica is removed than the chromium. Thus, the gate layer extends over the recesses of the insulator. This allows a line-of-sight path for the deposition of an iron catalyst layer directly on the silicon. The photoresist and excess iron are removed via a standard liftoff process using sonication in acetone. The CNTs are grown with chemical vapor deposition in a quartz furnace with methane, acetylene, and hydrogen [10].

Manuscript received June 11, 2010; revised August 11, 2010; accepted August 13, 2010. Date of publication September 13, 2010; date of current version November 5, 2010. This work was supported by DARPA under Contract HR0011-07-C-0056. The review of this paper was arranged by Editor W. L. Menninger.

L. T. Williams and M. L. R. Walker are with Georgia Institute of Technology, Atlanta, GA 30332 USA (e-mail: lwilliams@gatech.edu).

V. S. Kumsomboone and W. J. Ready are with Georgia Tech Research Institute, Atlanta, GA 30332 USA.

Color versions of one or more of the figures in this paper are available online at <http://ieeexplore.ieee.org>.

Digital Object Identifier 10.1109/TED.2010.2069563

TABLE I  
NOMINAL CNT ARRAY PATTERNS

Sample	Pattern Shape	Shape Size ( $\mu\text{m}$ )	Pitch ( $\mu\text{m}$ )	CNT Area ( $\text{cm}^2$ )
1	Triangle	4	16	0.0091
2	Diamond	8	64	0.0056
3	Diamond	2	8	0.0181
4	Star	8	32	0.0070
5	Star	50	150	0.0200
6	Diamond	1	8	0.0056
7	Square	4	16	0.0181

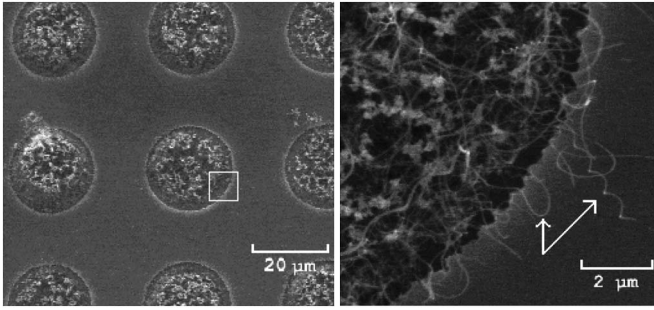


Fig. 1. Micrographs of CNT arrays. (Left) Near uniformity of arrays with the white outline denoting a zoomed-in image of (right) fringe CNTs, denoted by arrows near the edge of an individual array.

Fig. 1 shows images of circular CNT arrays from one of the samples created using this procedure, as well as a closer view of the nanotube morphology obtained with a scanning electron microscope. The arrays demonstrate a degree of overall uniformity, although there is slight variation between some arrays. Fig. 1 also shows a presence of fringe nanotubes that do not conform to the overall shape of the arrays. The individual nanotubes that make up the arrays have an outer diameter of about 20 nm. The density of the nanotubes within each array is about 10% by area, which means that each nanotube is about 70 nm apart. Despite the overall structure of the CNT arrays, the individual nanotubes display a kinked vinelike morphology and have a degree of anisotropy [10].

The process used in this work created nanotubes that visibly extend beyond the gate, as shown in Fig. 1. The resultant arrays have a height of about 50  $\mu\text{m}$ , rather than the expected 5–10  $\mu\text{m}$ . This requires the addition of an external gate suspended above the surface of the wafer to extract electrons. An electric field applied across this external gate and the CNT arrays extracts the electrons rather than the chromium gate as anticipated. For the rest of this paper, the chromium gate is ignored and left electrically floating.

The wafer that contains the CNT arrays is mounted on an aluminum body with Pelco colloidal silver liquid. The gate is a 0.035-mm-thick molybdenum grid with 0.14-mm hexagonal holes with a 0.025-mm edge-to-edge separation and a total transparency of 71.6%. The gate is mounted 1.3 mm above the surface of the wafer with an anode placed 2.5 cm further.

### B. Experimental Apparatus

All experiments are conducted in a 0.5-m-diameter 0.7-m-tall stainless-steel bell jar vacuum system. The bell jar is evacuated with a Varian VHS-6 diffusion pump that is mechanically

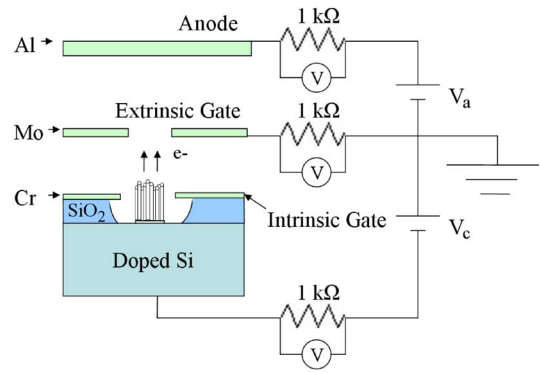


Fig. 2. Cathode electrical schematic.

backed by an Alcatel 2033 SD rotary vane pump. An uncooled optical baffle prevents oil from backstreaming into the bell jar. The diffusion and backing pumps have pumping speeds (for air) of 2400 and 8.33 L/s, respectively. Pressure in the bell jar is measured by a Bayard Alpert 571 ion gauge in connection with a SenTorr ion gauge controller with an overall error of 20% [11], as well as two Varian 531 thermocouple pressure transducers connected to Varian Model 801 thermocouple gauge controllers.

Fig. 2 shows the triode configuration used to connect the cathode, gate, and anode. The anode bias voltage  $V_a$  is supplied by a Xantrex XPD 60-9 power supply. The cathode bias voltage  $V_c$  is supplied by a Kepco BHK 2000-0.1MG power supply. The negative of the anode supply and the positive of the cathode supply are grounded together with the gate in a triode configuration. The currents to the gate, anode, and cathode are measured across three 1-k $\Omega$  current shunts with a combination of a Fluke multimeter and an Agilent 34970A data acquisition unit (DAQ). The resistance value has a tolerance of  $\pm 5\%$ , the multimeter has an uncertainty of 0.1%, and the DAQ has an uncertainty of 0.004%. The resistors have a temperature coefficient of 260 ppm/ $^{\circ}\text{C}$ ; considering that the ambient temperature can range from 6 to 27  $^{\circ}\text{C}$ , this adds an additional +0.052/–0.494% uncertainty to the resistance.

### C. Procedure

Each sample is individually tested in the bell jar vacuum system. The chamber is evacuated to a pressure below  $10^{-5}$  T. The anode is biased to 50 V, and the cathode voltage is progressively increased in 50 V steps at 5-min intervals to a set voltage for each sample, at which point the cathode potential is held constant. Sample 1 is held at 1075 V; sample 2 is held at 1400 V; samples 3, 5, 6, and 7 are held at 1200 V; and sample 4 is held at 1000 V. Once the cathode potential is at the final voltage, the current is measured every 5 min until the cathode ceases to emit. The average current density is calculated as the current output divided by the area of the cathode occupied CNT arrays.

## III. RESULTS

Fig. 3 shows the current density emitted by each cathode sample over time. One common characteristic among all of the current emission traces of the samples over time is the existence

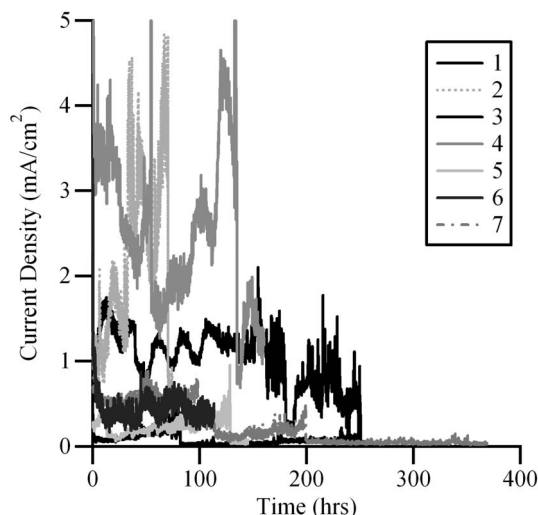


Fig. 3. Summary of CNT cathode emission current density over time.

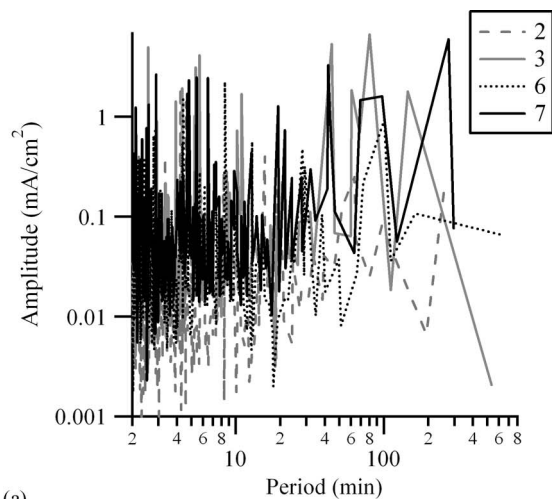
TABLE II  
CNT PERFORMANCE STATISTICS

Sample	Life (hrs)	Max Current Density (mA/cm <sup>2</sup> )	Median Current Density (mA/cm <sup>2</sup> )	Mean Current Density (mA/cm <sup>2</sup> )	Standard Deviation (mA/cm <sup>2</sup> )
1	250	2.10	1.35	1.34	0.24
2	83	4.83	1.84	1.95	1.11
3	249	0.50	0.06	0.08	0.06
4	117	9.08	2.44	2.52	1.04
5	145	0.95	0.23	0.22	0.11
6	113	0.44	0.42	0.44	0.18
7	368	1.54	0.05	0.18	0.22

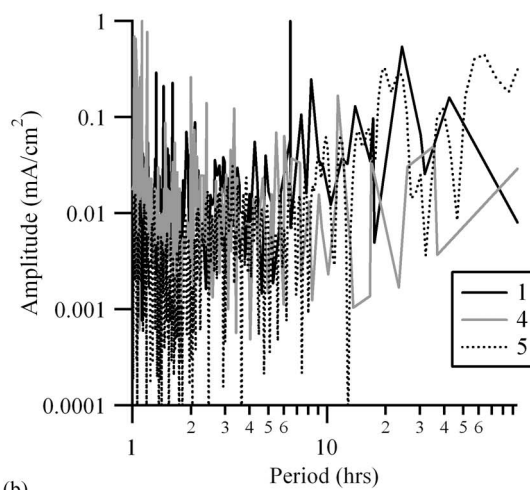
of discontinuous jumps in the current emission, particularly just before the sample fails. Some samples demonstrated multiple shifts in current emission, such as samples 2, 3, 4, and 7. Table II shows a summary of the performance statistics of the samples in terms of the cathode lifetime and the mean, median, maximum, and standard deviation of the current density emitted.

Another major characteristic of the measured current densities is that many have an oscillatory nature. Samples 1 and 4 both have what appears to be a single dominant oscillation combined with a slowly changing dc component, whereas samples 2 and 6 have a sum of several oscillations at different frequencies combined with a dc component. In order to make a more definitive comparison, the data sets were processed with a power spectrum algorithm that utilizes Prony's method [12]. Sample 5 had an instrument error that caused the data collection to occur at irregular intervals, which required the use of Lomb-Scargle periodogram analysis, instead of Prony's method.

Fig. 4 shows the results of the signal analysis of the current emission. The amplitudes of the spectra are normalized by the mean current density emitted by each sample for the sake of comparison, and the amplitudes are presented as a function of the period of the oscillation. Samples 1, 3, 5, and 7 all seemed to have a combination of long- and short-period components to their oscillations, whereas samples 2, 4, and 6 were mostly short-period oscillations. The values at which these longer period spikes occur correspond to oscillations occurring with a period on the order of hours, which agrees with the observed data.



(a)



(b)

Fig. 4. Power spectra of cathode current emission density. (a) Samples with a sampling period of 600 s. (b) Samples with a sampling period of 30 s or an irregular sampling period.

Continuing this line of examination, the seven plots are normalized and arranged according to similarities. Fig. 5 shows the current emission of each cathode normalized by the maximum recorded value and plotted against normalized time. Doing so, several interesting observations can be made. First, the similarities based on spectral comparisons in frequency space hold when comparing the plots in time space; that is, samples with similar frequency spikes have similar plot shapes. Second, between samples 2, 4, and 5, each cathode experienced a sudden drop in current emission at about 85% of the total lifetime. This is similar to sudden shifts or changes in current emission experienced by samples 3 and 7, except that they occurred multiple times.

#### IV. DISCUSSION

The first observation of importance is the unsteady behavior of the cathode current emission over time. This lack of stability conforms to observations seen in similar work under certain circumstances and suggests that the partial pressure of water vapor is a decisive parameter. The second observation of note is the mechanism for the failure of the cathodes. The relationship



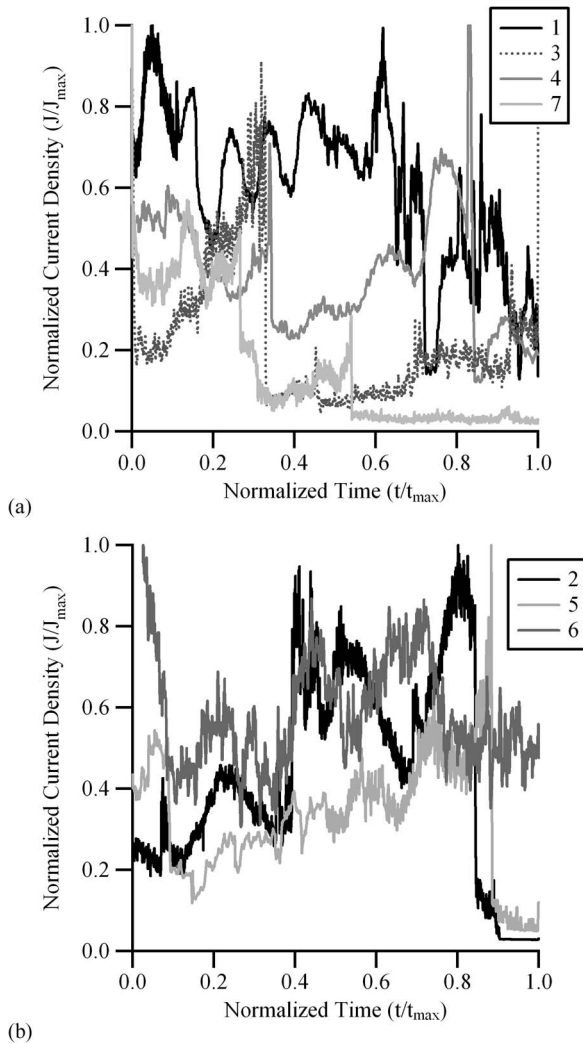


Fig. 5. Normalized current density as a function of normalized time at a constant voltage.

between the average cathode power density and cathode lifetime, along with observation of physical damage, suggests that the primary cause for failure is ohmic heating at two locations on the nanotubes. This difference in location for peak ohmic heating leads to two different modes of resistive failure.

#### A. Cathode Instability

Unlike the observed performance, most of the recent work on the stability of CNT cathode emission report much more stable emission. However, these reports can be considered as two sets: short- and long-duration testing. For short-duration testing (about half an hour), the observed current emission maintains a relatively steady value with minor perturbations in a manner similar to other work on vertically aligned nanotubes [13], [14]. After this initial period, the current begins to change more noticeably in no apparent pattern. This conforms somewhat to previous work [15]–[17] with some exceptions. First, Pandey *et al.* [15] observed overall a monotonic decrease in current emission over time, whereas here and in the other works, current emission both increased and decreased over time in equal proportions. Second, the observed changes in

current emission had large standard deviations ranging from slightly below 50% to over 100% of the mean. Data collected by Dean and Chalamala [16] and Aplin *et al.* [17] show a smaller deviation around the mean.

Further comparison to the other works does not reveal any clear reason for the instability. The behavior observed somewhat matches both Dean's and Aplin's reported emission over time despite the differences in nanotube composition. It is most probable that the instabilities are caused by the presence of water vapor in the vacuum chamber. Dean's research showed that SWNTs had an increase in instability when operated in an atmosphere containing water vapor. The experiments that had similar levels of instability (Aplin and Dean) ran at pressures only slightly below what is done in the current work, suggesting that higher partial pressures of water vapor is the common parameter. Pandey and Thong both operated at pressures two or three orders of magnitude below what is observed here, potentially mitigating the effects of the water vapor.

Even with the presence of water vapor as a potential cause, the magnitudes of the oscillations are much larger than that seen by Dean at a similar pressure. It is possible then that the irregular behavior of the current emission is due to some form of motion of the nanotubes within the arrays or within the nanotubes themselves. Current switching can be caused by motion of the nanotube, as different facets of the CNT structure have slightly different work functions. Collins and Zettl show that current switching caused by interactions between nanotubes could shift current emission by an order of magnitude in only a few seconds [18]. The problem with this theory and with nanotube motion as the cause in general is that signal analysis resulted in periods on the order of hours or days, which give frequencies on the order of millihertz and microhertz. While these frequencies do correspond to the oscillations observed, most recorded nanotube motion is on the frequency scale of megahertz to gigahertz [19], [20] and thus is too fast to be responsible for the observed behavior. Another possibility is that the anomalously long nanotubes are the cause of emission instability. This is also unlikely, as work by Thong *et al.* [13] used nanotubes of a similar length and did not observe the same manner of instability. For the sake of completeness, since shunt resistors are used, there is the possibility that the stray capacitance of the setup could affect the time resolution of the system. Calculations estimate the stray capacitance at about 20 pF, resulting in an RC time constant of about 6.5 ns, which is much smaller than the timescales already mentioned.

#### B. Failure Mechanism

Several observations can be made about the nature of cathode failure. The first is that scorch marks are readily apparent on the cathode surface of samples 1, 2, 4, and 7. Fig. 6 shows a compilation of optical microscope images of sample 4 that show regions of such scorching. Damage of this kind suggests that there are regions of high thermal deposition onto the surface of the wafer. These images also suggest oxidation along the surface of the wafer. The smaller reddish colorations on the surface of the wafer match the coloration of chromium oxide and are arranged in a hexagonal pattern matching the gate hole

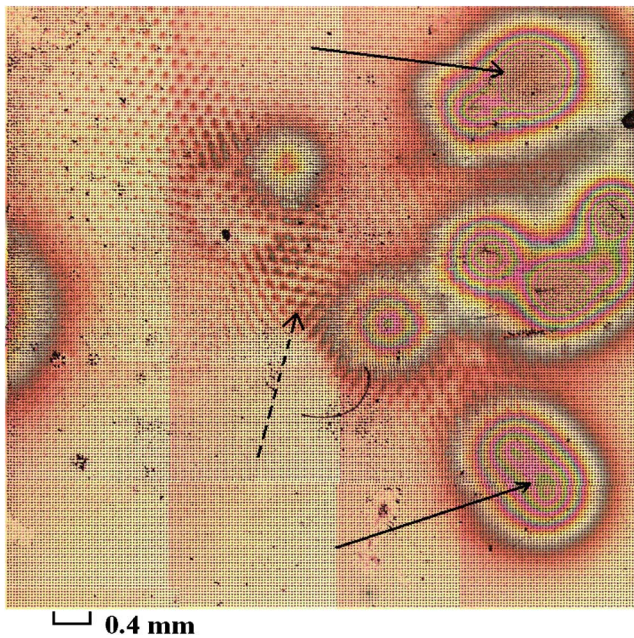


Fig. 6. Thermal damage on sample 4. Solid arrows point to the scorch marks, and dashed arrow points to one region of possible chromium oxide.

pattern. This suggests that the emitted electrons ionize residual oxygen molecules outside of the cathode; the resultant positively charged oxygen ions could then be accelerated through the gate into the surface of the wafer to form chromium oxide. It is worth noting that the strongest regions of such discoloration occur near the scorch marks.

The next observation is a comparison of the life test performance statistics. Since the scorch marks suggest some thermal process, it is enlightening to plot the cathode lifetime of each sample against the average power density through the cathode. Fig. 7 shows that there are two possible trends in the cathode lifetime: the first is a linear dependence ( $R^2$  of 0.994) with power density (consisting of samples 1, 2, 4, and 7), and the second is a probable exponential dependence ( $R^2$  of 0.895) with power density (consisting of samples 3, 5, and 6). While the low number of data points prevents anything definitive, this suggests that there are two failure mechanisms or at least two different modes of the same mechanism.

Considering the above, resistive heating is the most likely mechanism for failure. Resistive heating is the process where ohmic heating from the current passing through the nanotubes heats the tubes and enhances oxidative ablation, or outright vaporizes the outer wall [21]. Increasing the power density increases the rate at which the nanotubes capable of emission at a given electric field will be damaged beyond use. A point of note is that, after each test, the anode contains a film of dark brown material patterned in the magnified shape of the gate screen. This suggests that the material is most likely carbon that is vaporized and ejected from the cathode during operation. This suggests that, despite the two theorized modes of failure, they both involve the vaporization of carbon from the nanotubes.

From resistive heating, one can speculate that the two modes might arise from differences in the relative value of the contact

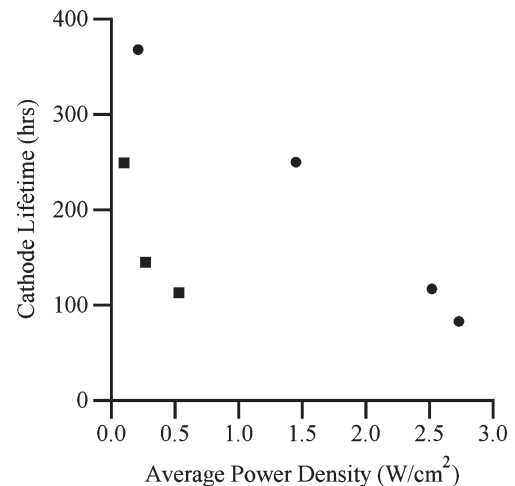


Fig. 7. Cathode lifetime as a function of the average power density of the cathode. Circle markers show linear dependence, and square markers show exponential dependence.

resistance. For nanotubes where the contact resistance between the nanotube and the substrate is much higher than the resistance of the nanotube, the majority of the ohmic heating is deposited at the root. The high temperatures enhance the rate of oxidative ablation and lead to the nanotubes rupturing near the root, leading to failure. The temperature at the contact resistance scales linearly with power, which matches the observations that samples 1, 2, 4, and 7 have large scorch marks and regions of oxidation and their lifetimes scale linearly with power density.

The second mode for resistive failure is when the resistance of the nanotube is higher than the contact resistance. In this situation, the peak temperature is found at the tip of the nanotube [21]. One observed phenomenon that can occur at the tip of a nanotube is field evaporation, which is analogous to FE, except that it is the removal of one or more atoms from the nanotube rather than electrons. Field evaporation generally requires very high electric fields beyond the scope of this experiment. However, as the temperature of the material increases, the rate of field evaporation increases exponentially and can be made nonnegligible over an extended period of time [22], [23]. The rate of field evaporation scales exponentially with temperature at the tip, which is linearly related to power deposition [21]. Thus, the lifetime of a cathode, which fails via field evaporation of the tip, should scale as an exponential decay. This correlates to the observation that samples 3, 5, and 6 have lifetimes that decay exponentially with power density and lack any surface scorching while still ejecting material onto the anode.

Resistive heating can lead to arcing, as the vaporized nanotube walls create a conductive path to the gate [21]. A region of sample 1 has solidified flow from melting the silicon substrate at the center of a scorch mark. The high temperature needed to melt silicon (1420 °C) combined with the quantity of molten silicon suggests that arcing occurred at that point, rather than some other phenomenon. Gröning *et al.* determined that arcing in a CNT film cathode could create currents of as high as  $8 \times 10^5$  mA/cm<sup>2</sup> in 200-ns pulses that could deposit  $10^4 - 10^5$  J/cm<sup>3</sup> of energy into the cathode [24]. Such an arc could

cause the observed damage, noting that a 200-ns pulse would not be registered by the DAQ unit. However, as the damage on sample 1 previously shown was the only case observed, arcing as a primary failure mechanism is rejected in favor of resistive heating.

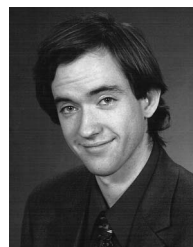
Another mechanism considered was failure due to mechanical stress. Failure caused by mechanical stresses is generally associated with CNT films, in which the nanotubes are not arranged in a given orientation and are forced into a vertical position by the applied electric field [21]. However, the cathodes here are operated at electric field intensities that are much lower than what was observed for failure ( $\sim 1$  V/ $\mu\text{m}$  versus 3 V/nm for previous work). It is worth stating that some fringe nanotubes in any given array may be more affected than the rest of the array, but this would not greatly impact overall emission due to the low number of fringe nanotubes.

## V. CONCLUSION

Seven CNT cathodes fabricated from vertically aligned arrays are operated with a constant voltage applied between the gate and CNTs over time to provide current densities of up to 9.08 mA/cm<sup>2</sup> and average current densities of up to 2.52 mA/cm<sup>2</sup> for lifetimes up to 368 h. The current emission over time is very unstable with behavior over time characterized by oscillations and sudden shifts potentially due to the presence of water vapor. Resistive heating is the probable cause of failure of the cathode, with two different modes: 1) thermally enhanced oxidative ablation at the root of the nanotube and 2) thermally enhanced field evaporation at the tip. The short cathode lifetime and unsteady emission fall short of the requirements for EP application, but refinement of the technology can make in-space use feasible.

## REFERENCES

- [1] J. Mueller, C. Marrese, J. Ziemer, A. Green, E.-H. Yang, M. Mojarradi, T. Johnson, V. White, D. Bame, R. Wirz, M. Tajmar, J. Schein, R. Reinicke, and V. Hruby, "JPL micro-thrust propulsion activities," presented at the NanoTech, Houston, TX, 2002, AIAA Paper 2002-5714.
- [2] W. A. Hargus, Jr. and G. Reed, "The air force clustered hall thruster program," presented at the 38th AIAA/ASME/SAE/ASEE Joint Propulsion Conf. Exhibit, Indianapolis, IN, 2002, AIAA Paper 2002-3678.
- [3] C. J. Gasdaka, P. Falkos, V. Hruby, M. Robin, N. Demmons, R. McCormick, D. Spence, and J. Young, "Testing of carbon nanotube field emission cathodes," presented at the 40th AIAA/ASME/SAE/ASEE Joint Propulsion Conf. Exhibit, Ft. Lauderdale, FL, 2004, AIAA Paper 2004-3427.
- [4] B. E. Gilchrist, K. L. Jensen, A. D. Gallimore, and J. G. Severns, "Space based applications for FEA cathodes (FEAC)," in *Proc. Mater. Res. Soc. Symp.*, 2000, vol. 621, pp. R481–R487.
- [5] C. A. Spindt, C. E. Holland, A. Rosengreen, and I. Brodie, "Field-emitter arrays for vacuum microelectronics," *IEEE Trans. Electron Devices*, vol. 38, no. 10, pp. 2355–2363, Oct. 1991.
- [6] V. M. Agüero and R. C. Adamo, "Space applications of Spindt cathode field emission arrays," in *Proc. 6th Spacecr. Charging Technol. Conf.*, Bedford, MA, 1998, pp. 347–352.
- [7] W. A. de Heer, A. Chatelain, and D. Ugarte, "Carbon nanotube field-emission electron source," *Science*, vol. 270, no. 5239, pp. 1179–1180, Nov. 1995.
- [8] M. Gamero-Castaño, V. Hruby, P. Falkos, D. Carnahan, and B. Ondrusek, "Electron field emission from carbon nanotubes, and its relevance in space applications," presented at the 36th AIAA/ASME/SAE/ASEE Joint Propulsion Conf., Huntsville, AL, 2000, AIAA Paper 2000-3263.
- [9] A. T. Sowers, B. L. Ward, S. L. English, and R. J. Nemanich, "Field emission properties of nitrogen-doped diamond films," *J. Appl. Phys.*, vol. 86, no. 7, pp. 3973–3982, Oct. 1999.
- [10] S. P. Turano and W. J. Ready, "Chemical vapor deposition synthesis of self-aligned carbon nanotube arrays," *J. Electron. Mater.*, vol. 35, no. 2, pp. 192–194, 2006.
- [11] "Vacuum Measurement," Varian, Inc., Palo Alto, CA, 2003.
- [12] S. M. Kay and S. L. Marple, "Spectrum analysis—A modern perspective," *Proc. IEEE*, vol. 69, no. 11, pp. 1380–1419, Nov. 1981.
- [13] J. T. L. Thong, C. H. Oon, W. K. Eng, W. D. Zhang, and L. M. Gan, "High-current field emission from a vertically aligned carbon nanotube field emitter array," *Appl. Phys. Lett.*, vol. 79, no. 17, pp. 2811–2813, Oct. 2001.
- [14] H. Murakami, M. Hirakawa, C. Tanaka, and H. Yamakawa, "Field emission from well-aligned, patterned, carbon nanotube emitters," *Appl. Phys. Lett.*, vol. 76, no. 13, pp. 1776–1778, Mar. 2000.
- [15] A. Pandey, A. Prasad, J. Moscatello, B. Ulmen, and Y. K. Yap, "Enhanced field emission stability and density produced by conical bundles of catalyst-free carbon nanotubes," *Carbon*, vol. 48, no. 1, pp. 287–292, Jan. 2010.
- [16] K. A. Dean and B. R. Chalamala, "The environmental stability of field emission from single-walled carbon nanotubes," *Appl. Phys. Lett.*, vol. 75, no. 19, pp. 3017–3019, Nov. 1999.
- [17] K. L. Aplin, B. J. Kent, W. Song, and C. Castelli, "Field emission performance of multiwalled carbon nanotubes for a low-power spacecraft neutralizer," *Acta Astronautica*, vol. 64, no. 9/10, pp. 875–881, May/June 2008, doi: 10.1016/j.actaastro.2008.10.012.
- [18] P. G. Collins and A. Zettl, "Unique characteristics of cold cathode carbon-nanotube-matrix field emitters," *Phys. Rev. B, Condens. Matter*, vol. 55, no. 15, pp. 9391–9399, Apr. 1997.
- [19] J. Cumings and A. Zettl, "Low-friction nanoscale linear bearing realized from multiwall carbon nanotubes," *Science*, vol. 289, no. 5479, pp. 602–604, Jul. 2000.
- [20] V. R. Coluci, S. B. Legoas, M. A. M. de Aguiar, and D. S. Galvão, "Chaotic signature in the motion of coupled carbon nanotube oscillators," *Nanotechnology*, vol. 16, no. 4, pp. 583–589, Mar. 2005.
- [21] J. Bonard and C. Klinker, "Degradation and failure of carbon nanotube field emitters," *Phys. Rev. B, Condens. Matter*, vol. 67, no. 11, pp. 115406-1–115406-10, Mar. 2003.
- [22] G. L. Kellogg, "Measurement of activation energies for field evaporation of tungsten ions as a function of electric field," *Phys. Rev. B, Condens. Matter*, vol. 29, no. 8, pp. 4304–4313, Apr. 1984.
- [23] K. A. Dean, T. P. Burgin, and B. R. Chalamala, "Evaporation of carbon nanotubes during electron field emission," *Appl. Phys. Lett.*, vol. 79, no. 12, pp. 1873–1875, Sep. 2001.
- [24] O. Gröning, O. M. Kuttel, E. Schaller, P. Groning, and L. Schlapbach, "Vacuum arc discharges preceding high electron field emission from carbon films," *Appl. Phys. Lett.*, vol. 69, no. 4, pp. 467–468, Jul. 1996.



**Logan T. Williams** (M'09) received the B.S. degree in mechanical engineering and the M.S. degree in aerospace engineering, in 2006 and 2009, respectively, from Georgia Institute of Technology, Atlanta, where he is currently working toward the Ph.D. degree in aerospace engineering.

He is currently a Graduate Researcher with Georgia Institute of Technology. His current research includes carbon nanotube field emission cathodes and helicon plasma sources.

Mr. Williams is a Student Member of the American Institute of Aeronautics and Astronautics.

**Victor S. Kumsomboone**, photograph and biography not available at the time of publication.

**W. Jud Ready** (SM'09), photograph and biography not available at the time of publication.

**Mitchell L. R. Walker**, photograph and biography not available at the time of publication.